processes

MDPI

Article

Synergetic Adsorption of Dyes in Water by Three-Dimensional Graphene and Manganese Dioxide (PU@RGO@MnO_2) Structures for Efficient Wastewater Purification

Shirong Zong [1,2], Jijun Jiang [1], Guodong Wang [1,*], Jin Zhong [1], Chunlan Tang [1], Lingxiang Zhou [1], Fan Yang [1] and Wei Yan [2]

[1] Yannan Yuntianhua Co., Ltd., Kunming 650228, China
[2] Department of Environmental Science and Engineering, School of Energy and Power Engineering, Xi'an Jiaotong University, Xi'an 710049, China
* Correspondence: wanggd0221@163.com

Abstract: The improper discharge of industrial wastewater causes severe environmental pollution and the textile industry's dye usage contributes significantly to industrial wastewater pollution. Hence, an effective method for removing the harmful substance methylene blue (MB) from dye wastewater is proposed. This method adopts a three-dimensional graphene composite material based on manganese dioxide (MnO_2), named polyurethane@ reduced graphene oxide@ MnO_2 (PU@RGO@MnO_2). First, graphene is prepared with hydrazine hydrate as a reducing agent and polyurethane as a framework. MnO_2 nanoparticles are synthesized by the reaction of potassium permanganate ($KMnO_4$) with carbon. These nanoparticles are then loaded onto the three-dimensional framework to create the composite material. Finally, adsorption and removal experiments for MB are conducted to compare the performance of the composite material. The results indicate that the graphene based on the polyurethane framework exhibits favorable mechanical properties. The unique three-dimensional lattice structure provides abundant active sites for loading MnO_2 nanoparticles, significantly increasing the contact area between the adsorbent and MB solution and thus improving the adsorbent utilization rate (reaching 94%). The nanoparticles synthesized through the reaction of $KMnO_4$ with carbon effectively suppress the agglomeration phenomenon. Additionally, the introduction of dynamic adsorption and dynamic removal modes, aided by a water pump, substantially enhances the adsorption and removal rates, showcasing excellent performance. The research on a multi-porous three-dimensional structure holds significant practical value in water treatment, offering a new research direction for dye wastewater treatment.

Keywords: wastewater treatment; water purification; adsorption; three-dimensional graphene; manganese dioxide

Citation: Zong, S.; Jiang, J.; Wang, G.; Zhong, J.; Tang, C.; Zhou, L.; Yang, F.; Yan, W. Synergetic Adsorption of Dyes in Water by Three-Dimensional Graphene and Manganese Dioxide (PU@RGO@MnO_2) Structures for Efficient Wastewater Purification. *Processes* **2024**, *12*, 169. https://doi.org/10.3390/pr12010169

Academic Editors: George Z. Kyzas and Monika Wawrzkiewicz

Received: 14 September 2023
Revised: 15 November 2023
Accepted: 20 December 2023
Published: 10 January 2024

1. Introduction

In modern industrial society, the improper discharge of industrial wastewater has become one of the major contributors to severe environmental pollution [1]. This is particularly evident in the textile industry, where the extensive use of dyes leads to the discharge of large quantities of dye-containing wastewater, including harmful dyes like methylene blue (MB) [2]. These hazardous substances pose a potential threat to aquatic ecosystems and human health. Therefore, the advancement of efficient and environmentally friendly wastewater treatment technologies has become a top priority. In order to address this issue, this work explores the preparation and application of a three-dimensional (3D) graphene composite material based on manganese dioxide (MnO_2), known as polyurethane@ reduced graphene oxide@ MnO_2 (PU@RGO@MnO_2), to achieve efficient purification of dye wastewater. Graphene, MnO_2, and polyurethane (PU) serve as the core components of the material and possess unique properties that make them powerful tools for handling

harmful substances in wastewater. With a high surface area and excellent conductivity, graphene performs remarkably well in adsorption and electrocatalytic reactions [3]. MnO_2, known for its outstanding oxidative capabilities, can effectively degrade dyes [4]. PU, as the framework of the composite material, provides mechanical stability and offers more active sites, aiding in the dispersion and immobilization of carrier nanoparticles [5]. This distinctive composite material structure provides a novel approach to removing harmful substances from wastewater.

The applications of graphene, MnO_2, and PU in the field of wastewater treatment have gained significant attention. Graphene's high surface area and conductivity bestow upon it exceptional adsorption and electrocatalytic characteristics, making it an ideal material for wastewater purification [6]. Meanwhile, MnO_2 is highly regarded for its excellent oxidative performance as it can effectively degrade hazardous organic compounds in wastewater, including dyes [7]. Furthermore, the role of PU in composite materials should not be underestimated. Serving as the framework of composite materials, it provides feasibility for loading nanomaterials while maintaining good mechanical properties [8], making PU an ideal choice for constructing PU@RGO@MnO_2 composite materials.

Currently, in China, commonly used methods for wastewater treatment include advanced oxidation, adsorption, biological treatment [9], electrochemical treatment [10], coagulation and precipitation, membrane technology, and high-temperature deep oxidation [11]. The advanced oxidation and adsorption are the most widely used. Advanced oxidation aims to oxidize non-degradable, difficult-to-degrade, and toxic organic pollutants under environmental conditions. Besides industrial wastewater treatment, it can also be applied in residential drinking water treatment [12]. The primary advantage of adsorption in wastewater treatment lies in its relatively low cost and high removal efficiency. Adsorbents capture harmful substances through intermolecular forces on the surface of the adsorption material, followed by further treatment to achieve the purification of water resources [13].

This work proposes a wastewater treatment material based on MnO_2, which offers advantages like relatively low cost, non-toxicity, and excellent adsorption and catalytic effects. MnO_2 tends to agglomerate when used individually, leading to a reduction in its specific surface area and a decrease in adsorption and catalytic efficiency. Hence, unlike previous research, this work aims to combine MnO_2 with graphene and PU to create a composite material with a multi-level pore structure called PU@RGO@MnO_2. This novel composite material exhibits exceptional performance in wastewater treatment, offering a new solution for wastewater purification. Therefore, the research originality lies in the combination of MnO_2 with graphene and PU, resulting in an efficient wastewater treatment material. This material has the potential to advance wastewater treatment technologies and achieve more sustainable wastewater purification methods.

2. Research Methods

2.1. Preparation of MnO_2

The preparation of MnO_2 primarily includes three categories: a hydrothermal process, a low-temperature solid-phase synthesis, and a chemical precipitation method.

The hydrothermal process [14] involves using water as the solvent for the reaction, in which the reactants are placed in a hydrothermal synthesis reactor and subjected to a constant temperature reaction in a heating device. This method effectively prevents issues related to uneven crystallization and impurity mixing. However, it has the drawback of requiring high temperatures, strict reaction conditions, and increased reaction costs.

The low-temperature solid-phase synthesis [15] is the process of grinding solid reactants together at low temperatures to obtain the desired products. The advantage is that the reaction can occur at relatively low temperatures, avoiding the crystal agglomeration issues associated with high-temperature reactions. However, the high requirement of MnO_2 for grinding may result in less controllable product outcomes, limiting the applicability of this method.

The chemical precipitation method [16] involves converting metal salt reactants into metal oxide precipitates under specific conditions, forming nanoparticles. Its main advantages are the lower requirement for reaction conditions and lower reaction costs. The most commonly adopted method is the redox process, which uses potassium permanganate ($KMnO_4$) and carbon to undergo an oxidation-reduction reaction to obtain MnO_2 nanoparticles. This method offers simple operation, easy access to reaction materials, and practical utility.

2.2. Preparation of PU@RGO@MnO_2

2.2.1. Experimental Materials and Equipment

Table 1 denotes the raw materials and reagents required in the experiment:

Table 1. Experimental Materials and Reagents.

Raw Materials and Reagents	Specification	Manufacturers
$KMnO_4$	Analytically pure	Beijing Chemical Works, Beijing, China
Oil of vitriol	Analytically pure	Beijing Chemical Works, Beijing, China
Sodium nitrate	Analytically pure	Xilong Chemical Company, Guangdong, China
Concentrated hydrochloric acid	Analytically pure	Beijing Chemical Works, Beijing, China
PU Sponge	0.5 m × 0.5 m	Hebei Warner Bros, Hebei, China
Flake natural graphite	300 Mesh	East China Graphite Factory, Guangdong, China
Hydrogen peroxide	30%	Beijing Chemical Works, Beijing, China

Table 2 indicates the equipment required in the experiment:

Table 2. Experimental Installation.

Instrument	Specification	Manufacturers
Analytical balance	AP135W	Shimadzu, Tokyo, Japan
IKA stirring hot stand	RET	Germany IKA, Staufen, Germany
Ultrasonic cell crusher	JY92-IIDN	Njinbo Scientc Biotechnology Co., Ltd., Zhejiang, China
Blast drying oven	DHG-9050A	Beijing Luxi Technology Co., Beijing, China
Desk centrifuge	TG16-WS	Hunan Xiangyi Laboratory Instrument Company, Xiangtan, China
Magnetic stirring apparatus	RO-10POWER	Shanghai Zhenrong Instrument Company, Shanghai, China
Vacuum drying chamber	DZF-6050	Beijing Luxi Technology Co., Beijing, China

2.2.2. Flowchart of the Experiment

Figure 1 presents the flow chart of the preparation of 3D composites.

2.2.3. Preparation Method of PU@RGO@MnO_2

- The graphene oxide (GO) was prepared by the water bath method. Then, the prepared GO was centrifugally washed with a centrifugal pump and then prepared into a GO solution with a concentration of 3 mg mL^{-1}. (RGO stands for reduced graphene oxide, which is a material obtained from GO after reduction treatment).
- The reducing agent in the experiment was hydrazine hydrate (HHA), which was mixed with the above-prepared GO in a ratio of 1:1, and ultrasonically cleaned for 20 min. The cleaned samples were ultrasonically pulverized with an ultrasonic cell pulverizer for 20 min, and the reducing agent and GO were mixed uniformly for later use.

- A PU sponge was added to the mixed solution in step 2 to make it completely submerged, putting it in a blast drying oven for 5 h at 65 °C, and drying the product at 75 °C in a blast drying oven to obtain a composite material PU@ RGO.
- A $KMnO_4$ solution with a concentration of 10 mg mL^{-1} was prepared and the PU@RGO obtained above was added to the solution and placed in a vacuum environment to completely immerse the PU@RGO in $KMnO_4$. Then, it was heated and reacted in a water bath at 80 °C for 20 min, and the reacted product was washed with deionized water. After washing, it was placed in a blast drying oven and dried at 75 °C to obtain the final composites PU@RGO@ MnO_2.

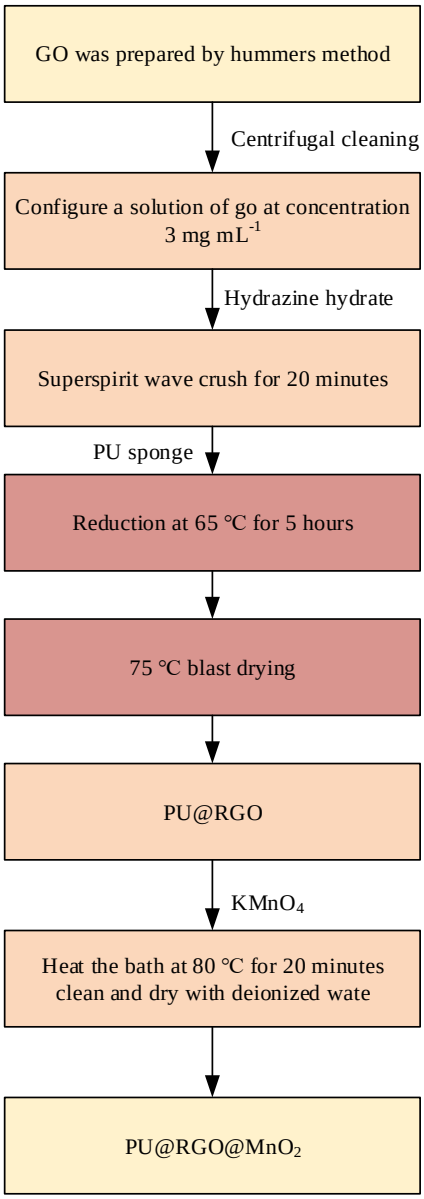

Figure 1. Experimental flow graph.

2.3. Analysis Methods

X-ray diffraction (XRD) [17] is a technique that employs X-rays to diffract and analyze the sample to obtain the sample's composition, molecular structure, and atomic structure. It is primarily used to analyze the crystal structure of the sample. X-ray photoelectron spectroscopy (XPS) [18] can analyze the sample's molecular structure and atomic valence state and its elemental composition and chemical bond. Raman spectra [19] mainly explore the information of molecular vibration and rotation by scattering spectra with different

frequencies from the incident light. It is primarily utilized to characterize the degree of reduction of reduced graphene oxide. A thermo-gravimetric analysis (TGA) [20] is employed to determine the component content of the samples.

The residual dye in the MB solution is examined using a UV-Vis spectrophotometer, and its adsorption is tested. The calculation of adsorption efficiency [21] reads:

$$f = \frac{C_0 - C_t}{C_0} \times 100\% \quad (1)$$

The initial concentration of MB is denoted by C_0, and the MB concentration at any time is denoted by C_t.

The equation for the adsorption capacity of pollutants reads:

$$Q_t = \frac{(C_0 - C_t)V}{m} \quad (2)$$

Q_t is the mass of pollutant adsorbed per unit of adsorbent. V is the volume of added pollutants, and m is the quantity of adsorbent.

The Bragg diffraction effect [22] refers to the fact that atoms have a scattering effect on X-rays, and the phase of the scattered rays in a specific direction is strengthened, which is called diffraction. The Bragg diffraction is exhibited in Equation (3):

$$2dsin\theta = n\lambda \quad (3)$$

The incident wavelength is λ, and d displays the spacing between the crystal planes. The incident angle and the angle between the incident light and the crystal plane are θ, and n represents the order of diffraction coherence.

2.4. Reaction Mechanism of Water Treatment of PU@RGO@MnO_2

The method of a simple adsorption machine cannot address these issues at the source and may still lead to environmental pollution. A conversion into clean substances is necessary to fundamentally solve these issues, which is vital in mitigating environmental pollution.

MnO_2 is a crucial element in the field of water treatment for two reasons. First, it exhibits a relatively strong adsorption capacity. Second, it serves as an excellent catalyst. When MnO_2 is used as a catalyst, only an oxidant needs to be added during the treatment process and it can convert MB into non-polluting small molecules through a chemical reaction. The oxidant used in the experiment is H_2O_2. MB is a cationic dye with positive charges on its surface. During the experiment, MnO_2 nanoparticles are generated through the redox reaction between RGO and $KMnO_4$ and these nanoparticles contain hydroxyl groups, making their surface have negative charges. For one thing, due to the negative charge of the nanoparticle, it interacts with the positive charge of MB and adsorbs it on the surface of the nanomaterial. For another, because of the presence of a benzene ring in the molecule of MB, it can form a π-π conjugated structure with graphene for adsorption, thereby achieving the effect of adsorbing dye molecules. In the experiment, adding H_2O_2 as an oxidant and MnO_2 as a catalyst, the H_2O_2 decomposes and generates a strong oxidizing hydroxyl group and other active free radicals.

In order to better understand the adsorption performance of the synthesized PU@RGO@MnO_2 material, a series of isothermal adsorption experiments are conducted. These experiments aim to evaluate the material's ability to adsorb specific substances under different conditions and study the influence of various factors on adsorption behavior. Isothermal adsorption experiments involve bringing the material into contact with a solution of the target substance and subsequently measuring the amount of adsorbed substance. Experiments are conducted under the following conditions: pH variation, salinity, and dissolved oxygen. Initially, a series of solutions containing the target substance are prepared and brought into contact with the PU@RGO@MnO_2 material. Isothermal adsorption exper-

iments are then conducted under different conditions for each experiment, recording the concentration changes of the material and the target substance after adsorption equilibrium. The solutions are prepared with specific target substance concentrations of 50 millimoles per liter. These solutions are used for both batch and continuous isothermal adsorption experiments. Batch experiments are conducted in a reactor with a volume of 250 milliliters, while continuous isothermal adsorption experiments are performed at a constant flow rate of 5 milliliters per minute. The catalyst loading of the PU@RGO@MnO_2 material is maintained at 2 milligrams to ensure consistency in experimental conditions. The concentration changes of the material and the target substance after adsorption equilibrium were recorded for each experiment. It's important to note that the wastewater mentioned here is an artificially prepared simulated liquid, not real wastewater from the environment. This decision is made for scientific research purposes, ensuring control over various parameters in the wastewater, such as target substance concentration, pH, and dissolved oxygen, to more accurately assess the performance of the studied material.

3. Results and Discussion

3.1. Microstructure Characterization

3.1.1. XRD Analysis

Through the above experiments, GO and 3D graphene PU@RGO@MnO_2 are successfully prepared. The XRD spectra of the two are obtained by XRD analysis, as exhibited in Figure 2:

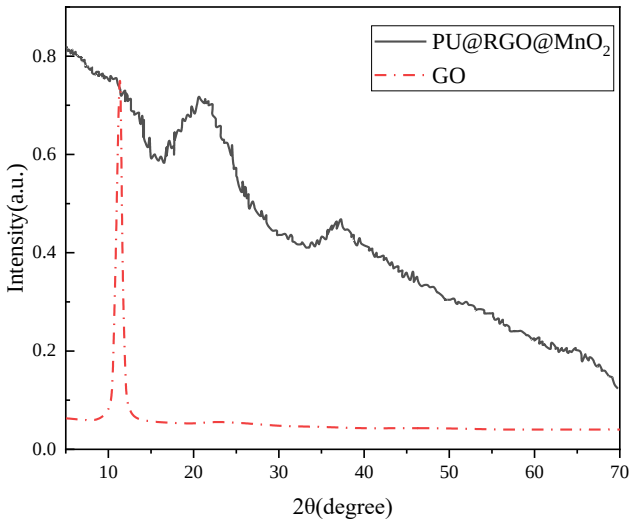

Figure 2. XRD patterns of GO and PU@RGO@MnO_2.

In Figure 2, although the original experimental data only include XRD analyses of GO and PU@RGO@MnO_2, these results can be compared with XRD data for RGO, MnO_2, and PU from previous literature. Hou et al. (2022) [23] extensively described the XRD analyses of RGO, MnO_2, and PU. By comparing the XRD spectrum of PU@RGO@MnO_2, broader crystalline peaks at 37° and 60° could be observed, indicating the presence of α-phase MnO_2 in PU@RGO@MnO_2. This is consistent with the results of Yang et al. (2022) [24], further confirming the successful synthesis of α-phase MnO_2.

For the XRD data of GO, a characteristic peak of the (001) crystal plane at 11.4° could be observed, and the lattice spacing was calculated to be 0.79 nm using the Bragg diffraction formula. Although direct XRD data for RGO is not provided, a comparison with the results of Hong et al. (2023) [25] suggests that characteristic peaks of RGO do not appear in PU@RGO@MnO_2. This phenomenon indicates that RGO undergoes etching reactions during the preparation of the composite material, further supporting the research conclusion.

The characteristic peak comparison demonstrates that the characteristic peaks in GO do not appear in PU@RGO@MnM_2, indicating the successful reduction of GO into RGO. However, since RGO is an intermediate substance and not the final product, the etching reaction occurs, so its corresponding characteristic peaks disappear and are not reflected in the XRD spectrum.

3.1.2. Raman Spectra

Raman spectra play a crucial role in characterizing carbon materials, with the D and G peaks commonly employed to assess the quality of carbon materials falling within specific ranges of Raman spectra. Among them, the D peak typically occurs near 1358 cm^{-1}, which represents the defect peak of the carbon material, mainly due to the formation of the disordered structure of the carbon material. The G peak results from the vibration of the C-C bond of sp2 hybridization, which can be applied to determine the degree of graphitization of carbon materials. The index often employed to measure the disorder degree of carbon materials is I_D / I_G. Figure 3 illustrates the specific Raman spectra:

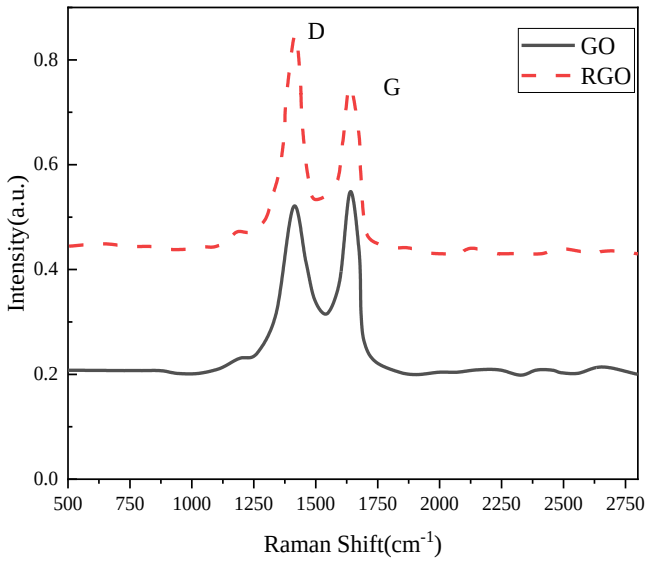

Figure 3. Raman spectra of GO and RGO. (The D peak represents the defect peak of carbon materials, while the G peak is used to determine the degree of graphitization of carbon materials.)

Figure 3 suggests that both the D and G peaks' positions in GO correspond to their respective positions before its reaction with the reducing agent, leading to the generation of RGO and GO. During this reaction process, oxygen functional groups in GO are successively removed. The removal of these oxygen functional groups results in more defects, leading to an increase in the I_D / I_G ratio, which provides evidence for the progress of the reduction reaction. This is why the intensity ratio of I_D / I_G for GO is 0.9, which is lower than the intensity ratio of 1.2 for I_D / I_G of RGO after reduction. This conclusion aligns with the findings of Ma and Xu (2022) [26].

3.1.3. Infrared Spectra Analysis

The sample should undergo infrared spectroscopy analysis to further determine the crucial components of the sample and determine its functional groups, as indicated in Figure 4:

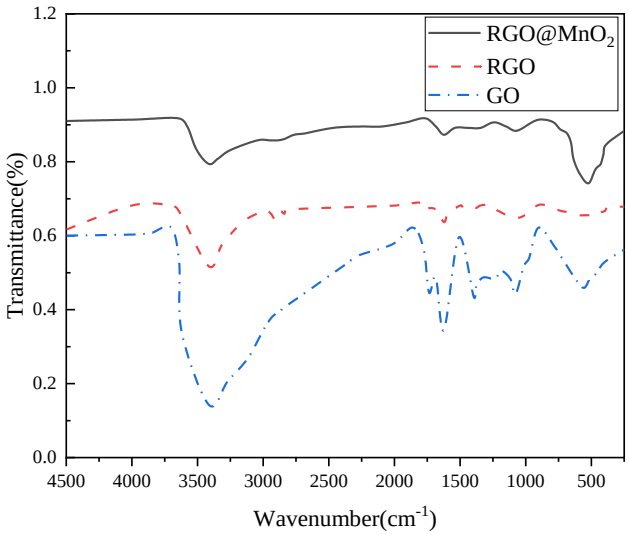

Figure 4. Infrared spectrogram of the GO, RGO, RGO@MnO_2.

In Figure 4, the absorption peak at 3413 cm^{-1} corresponds to the hydroxyl group's stretching vibration. The characteristic peak near 1732 cm^{-1} is attributed to the presence of carboxyl groups in GO, forming a characteristic peak due to the stretching vibration of C=O in the carboxyl group. The feature peak near 1622 cm^{-1} is associated with the bending vibration of C-OH, and the stretching vibration peak around 1076 cm^{-1} is a result of the vibration absorption of C-O-C. These observations indicate that the GO produced by the hydrothermal method contains numerous oxygen-containing functional groups, consistent with the results from the XRD spectrum. Additionally, Figure 4 reveals that the RGO generated with hydrazine as the reducing agent exhibits characteristic peaks of hydroxyl groups at approximately 1735 cm^{-1}, 1622 cm^{-1}, and 1076 cm^{-1}. These peaks have significantly lower absorption vibrations than GO. This reduction reaction leads to the removal of oxygen-containing functional groups. Furthermore, the infrared spectrum of RGO@MnO_2, compared to RGO, shows an additional absorption peak near 520cm^{-1}. This peak mainly results from the vibration of Mn-O bonds generated by the reaction-produced MnO_2. This firmly establishes that carbon reacted with $KMnO_4$ to form MnO_2, aligning with findings from Motaghi et al. (2022) regarding RGO research [27].

3.1.4. XPS Analysis

XPS analysis is conducted on the sample to further determine the elements constituting the sample and the existence form of the elements. Figure 5 demonstrates the results.

Figure 5a displays the spectrogram of RGO and RGO@MnO_2. The O and C peaks are clearly visible, indicating the presence of oxygen-containing functional groups in GO even after the reduction reaction. Compared with RGO, RGO@MnO_2 does not have C and O peaks, but has the corresponding characteristic peaks of Mn 2p, which proves the existence of MnO_2 in RGO@MnO_2. Figure 5b suggests that Mn $2p_{1/2}$ is at the position of 641.8 eV and Mn $2p_{3/2}$ is at the position of 653.5 eV. The difference between the two is 11.7 eV, which is consistent with the value in the MnO_2 data. It means that the load work for 3D graphene is realized. Their carbon peaks are further analyzed to ensure that GO has been successfully reduced to RGO. By comparing Figure 5c and Figure 5d, it is evident that in the spectrum of GO, C-C is at 285.7 eV, C-O-C is at 287.2 eV, C-O-H is at 286.5 eV and O-C=O is at 288.6 eV. Among them, although C-C is the main peak, the peaks of each oxygen-containing functional group are relatively strong. It fully proves that GO contains massive oxygen-containing functional groups. This conclusion aligns with the results from the XRD analysis. C-C still dominates the carbon peak of RGO and the peaks corresponding to oxygen-containing functional groups C-O-C, C-O=H and O-C=O are all weakened. In summary, it can be determined that GO has been converted into RGO and

the oxygen-containing functional groups are partially detached. The MnO_2 obtained by the redox reaction between the RGO produced by the reduction reaction and $KMnO_4$ is supported on the 3D graphene produced by the reduction of GO.

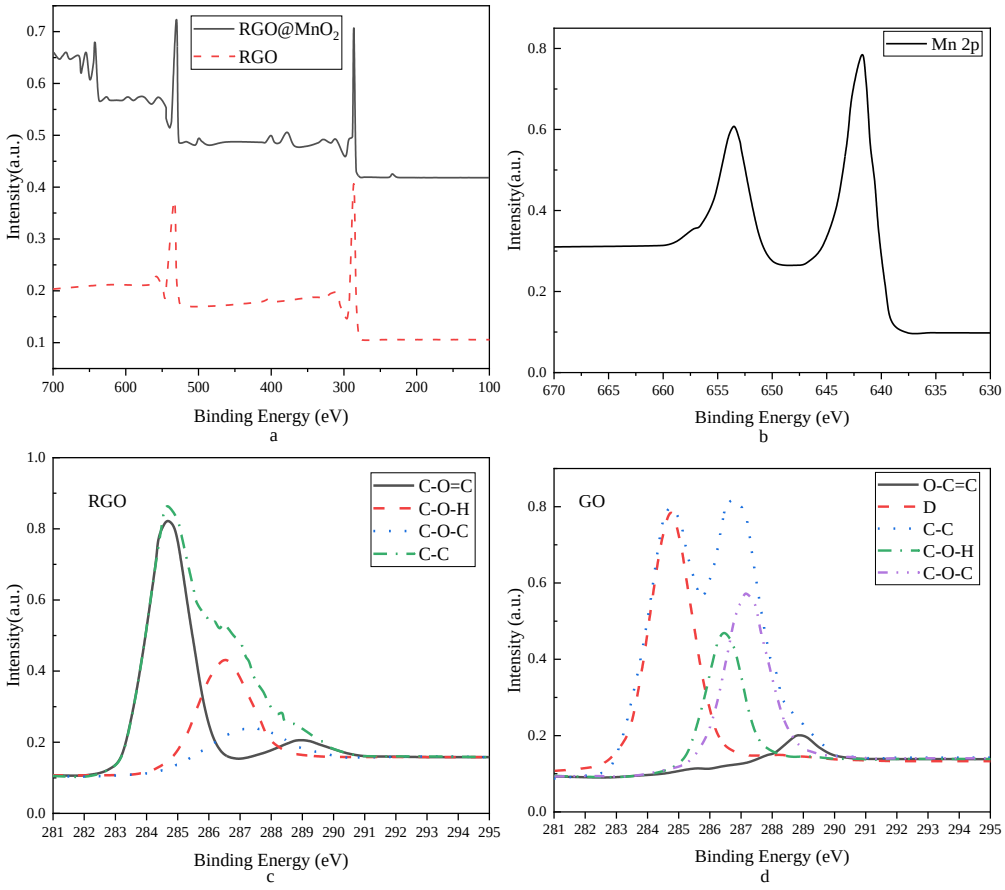

Figure 5. XPS graph of RGO and RGO@MnO_2. (**a**): represents RGO and RGO@MnO_2; (**b**): The amplification of Mn 2p; (**c**,**d**): The carbon peaks of X-ray photoelectron spectra of RGO and GO respectively.

3.1.5. TGA

The TGA of the PU sponge and the synthesized composites is carried out to further determine the specific content of MnO_2 in PU@RGO@MnO_2. Figure 6 demonstrates the specific situation.

In Figure 6, under atmospheric conditions, the temperature increases from room temperature to 800 °C at a rate of 10 °C per minute. Changes between the components of PU and PU@RGO@MnO_2 occurring as the temperature continuously rose are analyzed. There is a noticeable weight loss phenomenon for PU in the range of 250 °C to 350 °C. This is caused by the breaking of the PU main chain as the temperature increases. Furthermore, in the temperature range from 350 °C to 600 °C, the content continues to decrease due to an ongoing pyrolysis process. It stabilizes after 600 °C. The 3D composite material PU@RGO@MnO_2 undergoes weight loss due to the removal of crystalline water as the temperature increases. This conclusion aligns with the research results on 3D composite materials, as reported by Selvakumar et al. (2023) [28]. During the process from 180 °C to 400 °C, a significant increase in thermal weight loss occurs in the 3D composite material due to the combustion of RGO and PU. Finally, by comparing and analyzing the two TGA curves, it is estimated that the content of MnO_2 is approximately 26%.

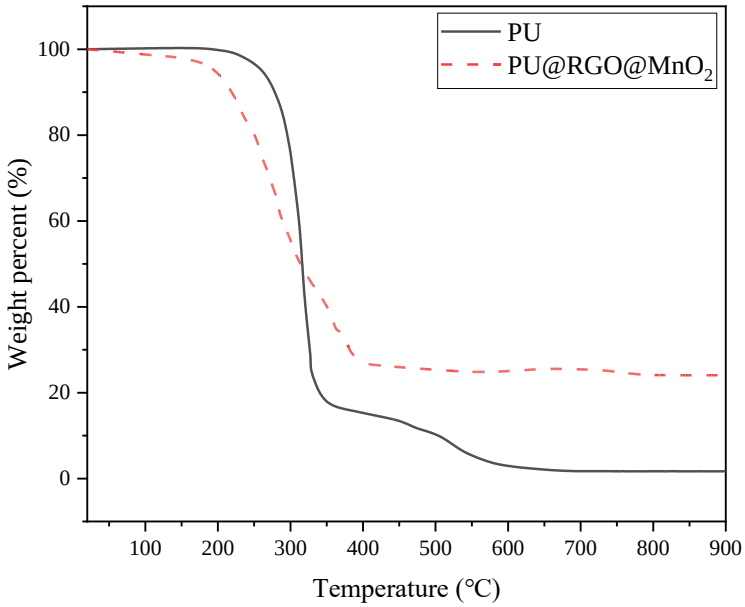

Figure 6. TGA plots for PU and PU@RGO@MnO_2.

3.2. Adsorption of MB by PU@RGO@MnO_2

The PU@RGO@MnO_2 solid adsorbent is added to the MB solution with an initial concentration of 50 ppm and the adsorption test is conducted. This test involved two modes: dynamic and static adsorption. The dynamic adsorption mode manifests the use of the unique hydrophilicity of the 3D material itself. The use of micro-pumps allows the liquid to pass through the adsorbent smoothly. This effectively utilizes the structural advantages of the 3D material's mesh, leading to an enhanced adsorption rate. Static adsorption involves placing a solid 3D material in a watch glass and simply relying on the random motion of the liquid molecules to make direct contact between the two to achieve the purpose of adsorption. Figure 7 illustrates the UV-Vis spectra of the two adsorption modes.

Figure 7a displays the UV-Vis spectrum of the static adsorption mode within 50 min. It is evident that the characteristic peak of MB at 665 nm is weakened but not obvious over time. Compared to the initial concentration, the change in concentration is minimal, suggesting that static adsorption relying on the liquid molecules' motion is ineffective. In order to solve this problem, it is compared with dynamic adsorption. The liquid can keep flowing continuously by using micro-pumps. It can reduce the problem of the poor adsorption effect caused by insufficient contact between the solid material and the liquid and expands the advantages of composite materials as much as possible. Figure 7b signifies that the value of the characteristic peak of MB has been in a decreasing trend with the increase of adsorption time. The decline is particularly obvious in the 10th minute. It basically stabilizes around the 20th minute, with almost no characteristic peaks at the 50th minute. The above results fully prove that dynamic adsorption is more effective than static and it fully utilizes the advantages of 3D composites. To further demonstrate the effect of dynamic superiority, the UV-Vis spectra of MB with initial concentration, PU, and PU@RGO after 50 min of adsorption are compared between the two adsorption modes. Both PU and PU@RGO are relatively high. The hydrophobicity of the MB solution hinders soaking adsorption experiments in the dynamic mode, so control experiments for PU and PU@RGO are conducted. Figure 7c denotes that there is almost no difference in the initial concentration and the peaks of the characteristic peaks of PU and PU@RGO during the whole experiment, indicating poor adsorption. While the peak value of the characteristic peak of PU@RGO@MnO_2-static has decreased, the effect is not obvious. The effect of PU@RGO@MnO_2-dynamic in the adsorption process is pronounced and the characteristic peaks change greatly and tend to disappear. It further proves that PU@RGO@MnO_2 has

the most effective adsorption, making it more valuable than other adsorption methods. The equations for calculating the adsorption efficiency given above are employed. The adsorption efficiencies of PU@RGO@MnO_2-dynamic, PU@RGO@MnO_2-static, PU@RGO, and PU are obtained. The adsorption efficiency of PU@RGO and PU is lower than 10% after 50 min, indicating poor adsorption effect. PU@RGO@MnO_2-static has a moderate improvement but still a relatively low adsorption rate, lower than 20%. Dynamic adsorption with the micro water pump significantly enhances the adsorption effect. PU@RGO@MnO_2-dynamic has reached equilibrium in 20 min and the adsorption efficiency exceeds 90% and finally reaches 94% after the test, which has obvious advantages compared with static adsorption. Compared to the study by Yang et al. (2023), the adsorption rate here is notably higher [29].

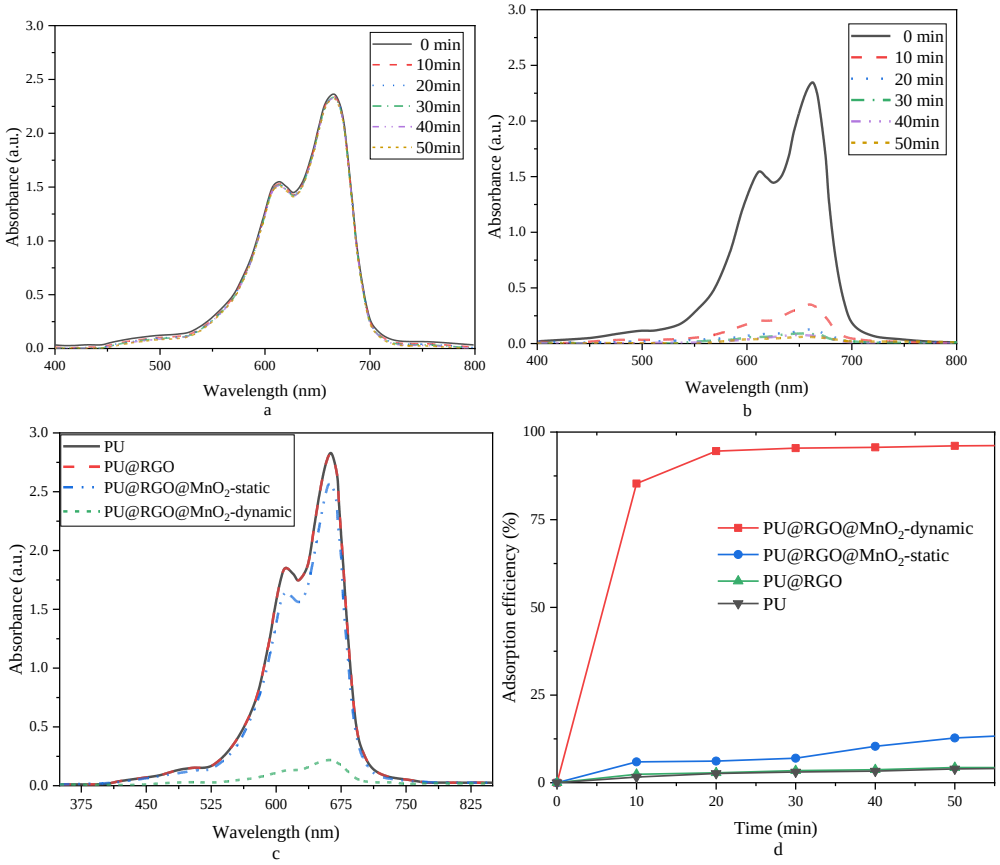

Figure 7. UV-Vis spectra of two adsorption modes. (**a**): Static adsorption UV-visible spectra; (**b**): dynamic adsorption mode UV-visible spectra; (**c**): Static adsorption mode 50 min UV-visible spectrogram; (**d**): Adsorption efficiency of the four substances at 50 min.

3.3. Removal of MBs Based on PU@RGO@MnO_2

During the experiment, the previous dynamic mode and static mode are employed. Different from the two modes of removal experiments of adsorption, the oxidant H_2O_2 is added in the experiment and MnO_2 is used as the catalyst. The static mode is the same as the static mode of the above adsorption experiment. It still relies on the disordered movement of the liquid molecules to promote contact between the solid material and the MB liquid. Figure 8 reveals the specific UV-Vis spectrum:

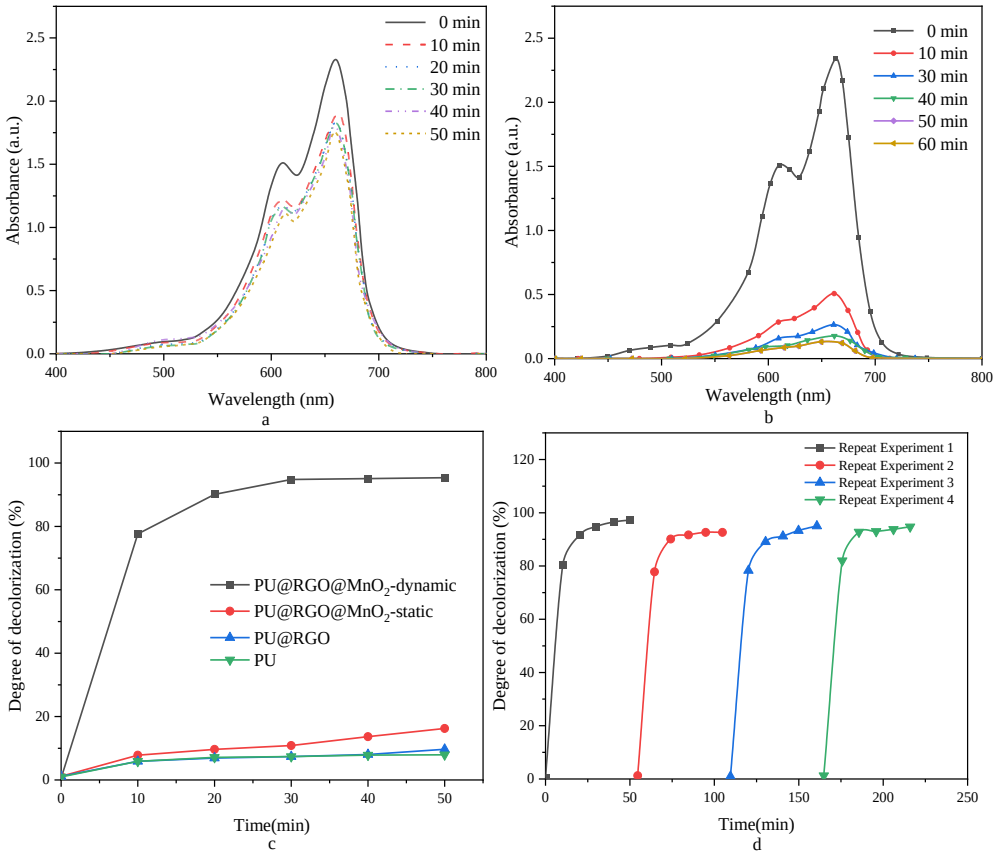

Figure 8. UV-VIS spectra of two removal modes. (**a**,**b**) are UV-vis spectra of PU@RGO@MnO_2-static and PU@RGO@MnO_2-dynamic removal experiments after 50 min, respectively. (**c**): Maps of PU, PU@RGO, PU@RGO@MnO_2-static and PU@RGO@MnO_2-dynamic removal efficiency at 50 min (**d**): PU@RGO@MnO_2-dynamic diagram of repeated test efficiency in PU@RGO@MnO_2-dynamic mode.

In Figure 8, the change of the peak is smaller with the increase of experimental time, indicating a poor removal effect. Figure 8b is the dynamic removal mode. It reveals that the peak value continuously decreases when the micro water pump is used due to the sufficient contact between the solid material and the MB liquid. It has reached equilibrium after 3 min, and there is almost no change after 30 min. Compared to the static removal mode, the effect is greatly enhanced. The removal efficiency is calculated using the adsorption efficiency equation. PU, PU@RGO, and PU@RGO@MnO_2-static are used as experimental controls to compare the removal efficiencies of various samples under different removal modes. Figure 8c demonstrates that there is almost no difference between the curves of PU and PU@RGO during the experiment and there is no major change even in the change of time. This fully illustrates that despite the addition of H_2O_2, there is no reaction, resulting in a poor effect. In PU@RGO@MnO_2-static, since MnO_2 can act as a catalyst to make H_2O_2 undergo a redox reaction, the removal efficiency has been improved to a certain extent. The removal efficiency of PU@RGO@MnO_2-dynamic is significantly improved, reaching 80% at 10 min, approaching 90% at 20 min, and finally achieving 96%. The removal effect is significantly higher than other substances. It is fully reflected that MnO_2 has a good adsorption effect and excellent catalytic effect. When the oxidant H_2O_2 is introduced, 3D composites demonstrate high applicability in the removal of MB. Figure 8d expresses the experimental efficiency of repeated use. It is apparent that the first removal efficiency has reached 96%. Although the effect of the subsequent three experiments is slightly reduced, the overall difference is not large and relatively stable. It is fully indicated that this material has good reusability and solid 3D composites offer distinct advantages in

practical applications with high application value. The removal efficiency here is higher compared to the study by Qu et al. (2022) [30].

3.4. Isothermal Adsorption Experiments

Table 3 presents the results of the isothermal adsorption experiments.

Table 3. The results of the isothermal adsorption experiments.

The Experimental Content		Adsorption Capacity (mg/g)
pH value	3	25.6
	5	31.2
	7	35.8
	9	29.7
Salinity (mS/cm)	2	28.5
	5	24.7
	10	21.3
	15	18.9
DO (mg/L)	1	24.6
	5	29.3
	10	33.1
	15	38.7

Table 3 demonstrates that the PU@RGO@MnO_2 material exhibits the highest adsorption performance at neutral pH (pH 7). This indicates that the adsorption performance may decrease under acidic or alkaline conditions. This result is crucial for selecting the most suitable environmental conditions to enhance adsorption performance. At lower salinity conditions, the PU@RGO@MnO_2 material shows a higher adsorption performance and, as salinity increases, the adsorption performance gradually decreases. This may be due to ion competition for adsorption sites under high salinity conditions, reducing the adsorption capacity of the target substance. With the increase in DO levels, the adsorption performance of the PU@RGO@MnO_2 material shows an upward trend, indicating that higher DO levels help improve adsorption efficiency. This conclusion is consistent with the research results on material adsorption performance in Zheng et al. (2022) [31].

4. Discussion

This work successfully synthesizes a 3D graphene composite material (PU@RGO@MnO_2) and extensively characterizes its performance. The primary components of the 3D graphene composite material include PU, RGO, and MnO_2. These components synergistically interact within the composite structure, offering the potential to remove harmful substances from water. First, RGO possesses a large surface area and abundant functional groups, endowing it with excellent adsorption capabilities to effectively adsorb organic and inorganic pollutants from water. Simultaneously, MnO_2, acting as an oxidant, can promote the oxidation and degradation of harmful substances. In an environmental context, the 3D structure of PU@RGO@MnO_2 provides more opportunities for contact, thereby enhancing the removal efficiency of pollutants. When harmful substances enter the porous structure of the composite material, the synergistic action of RGO and MnO_2 leads to the attachment and oxidation of these substances, effectively purifying the water. It is crucial to note that this mechanism is quite complex as it involves various reactions and interactions. Furthermore, water quality parameters such as pH, salinity, and DO also influence the performance of the composite material. Experimental results indicate that the PU@RGO@MnO_2 material has an excellent potential for removing harmful substances, which is crucial for water purification and environmental protection. This 3D composite material can achieve efficient adsorption and oxidative treatment for different contaminants in various water bodies. This is important for addressing wastewater treatment, purifying water resources, and mitigating environmental pollution issues. Additionally, this work provides valuable ex-

perience and insights for designing and preparing other novel composite materials with similar application potential.

5. Conclusions

This work involves preparing 3D graphene using PU as the framework of composite material and HHA as the reducing agent. MnO_2 nanoparticles are synthesized through redox reactions between $KMnO_4$ and carbon. These nanoparticles are then loaded onto the 3D framework to create the composite material. Finally, the PU@RGO@MnO_2 composite material absorbs and removes MB from the dye solution. It is found that graphene using PU as the framework exhibits good mechanical properties. Its unique 3D mesh structure provides ample active sites for MnO_2 nanoparticle loading, significantly increasing the contact area between the adsorbent and the MB solution and improving adsorbent utilization. The nanoparticles synthesized through the reaction of $KMnO_4$ with carbon effectively suppress the agglomeration phenomenon. The dynamic adsorption mode and dynamic removal mode, aided by the addition of a water pump, greatly enhance the adsorption and removal rates, demonstrating excellent performance. The multi-porous 3D graphene framework proposed holds significant research and application value in wastewater treatment. It is hoped that 3D graphene can gain widespread recognition and application in future water treatment research. The material's performance is influenced by water quality conditions, emphasizing the importance of environmental parameters. The practical significance of this work lies in the fact that environmental scientists and engineers can adjust and optimize the formulations and processes of these 3D graphene composite materials according to the needs of different application scenarios to achieve more efficient water quality treatment. It is worth noting that this work does not include BET and SEM analyses, but these are potential future research directions. Subsequent research can further analyze the material's microstructure and surface properties to better understand its performance.

Author Contributions: Conceptualization, S.Z. and J.J.; methodology, G.W. and W.Y.; validation, J.Z. and C.T.; formal analysis, L.Z.; investigation, G.W.; resources, C.T.; writing—original draft preparation, S.Z.; writing—review and editing, L.Z. and F.Y.; funding acquisition, G.W. All authors have read and agreed to the published version of the manuscript.

Funding: This research was funded by the Major Science and Technology Special Plan Project of Yunnan Province, grant number 202102AE090053.

Data Availability Statement: Data are contained within the article. The data are available upon request to the corresponding author.

Conflicts of Interest: S.Z., J.J., G.W., J.Z., C.T., L.Z. and F.Y. were employed by the Yannan Yuntianhua Co., Ltd. The remaining authors declare that the research was conducted in the absence of any commercial or financial relationships that could be construed as a potential conflict of interest.

References

1. Karaman, C.; Karaman, O.; Show, P.-L.; Orooji, Y.; Karimi-Maleh, H. Utilization of a double-cross-linked amino-functionalized three-dimensional graphene networks as a monolithic adsorbent for methyl orange removal: Equilibrium, kinetics, thermodynamics and artificial neural network modeling. *Environ. Res.* **2022**, *207*, 112156. [CrossRef]
2. Buu, T.T.; Son, V.H.; Nam, N.T.H.; Hai, N.D.; Vuong, H.T.; Dat, N.M.; Hieu, N.H. Three-dimensional ZnO–TiO_2/graphene aerogel for water remediation: The screening studies of adsorption and photodegradation. *Ceram. Int.* **2023**, *49*, 9868–9882. [CrossRef]
3. Ali, I.; Wan, P.; Raza, S.; Peng, C.; Tan, X.; Sun, H.; Li, J. Development of novel MOF-mixed matrix three-dimensional membrane capsules for eradicating potentially toxic metals from water and real electroplating wastewater. *Environ. Res.* **2022**, *215*, 113945. [CrossRef] [PubMed]
4. Fan, M.; Zhang, P.; Wang, C.; Tang, J.; Sun, H. Tailored design of three-dimensional rGOA-nZVI catalyst as an activator of persulfate for degradation of organophosphorus pesticides. *J. Hazard. Mater.* **2022**, *428*, 128254. [CrossRef] [PubMed]
5. Gupta, A.D.; Kirti, N.; Katiyar, P.; Singh, H. A critical review on three-dimensional cellulose-based aerogels: Synthesis, physicochemical characterizations and applications as adsorbents for heavy metals removal from water. *Cellulose* **2023**, *30*, 3397–3427. [CrossRef]

6. Abdelhamid, H.N.; Sultan, S.; Mathew, A.P. Binder-free Three-dimensional (3D) printing of Cellulose-ZIF8 (CelloZIF-8) for water treatment and carbon dioxide (CO_2) adsorption. *Chem. Eng. J.* **2023**, *468*, 143567. [CrossRef]
7. Anjum, M.; Liu, W.; Qadeer, S.; Khalid, A. Photocatalytic treatment of wastewater using nanoporous aerogels: Opportunities and challenges. *Emerg. Tech. Treat. Toxic Met. Wastewater* **2023**, *2023*, 495–523.
8. Solukluei, F.H.; Hassani, A.H.; Moniri, E.; Panahi, H.A.; Shirazi, R.H.S.M. Novel three-dimensional graphene oxide modified with hyper-branched dendrimer for removal of cephalexin from aqueous solutions by applying Taguchi statistical method. *Inorg. Chem. Commun.* **2023**, *148*, 110308. [CrossRef]
9. Gildernew, E.; Tareq, S.; Yang, S. Three-Dimensional Graphene with Preserved Channeling as a Binder Additive for Zeolite 13X for Enhanced Thermal Conductivity, Vapor Transport, and Vapor Adsorption Loading Kinetics. *Catalysts* **2022**, *12*, 292. [CrossRef]
10. Singh, R.; Ullah, S.; Rao, N.; Singh, M.; Patra, I.; Darko, D.A.; Issac, C.P.J.; Esmaeilzadeh-Salestani, K.; Kanaoujiya, R.; Vijayan, V. Synthesis of three-dimensional reduced-graphene oxide from graphene oxide. *J. Nanomater.* **2022**, *2022*, 8731429. [CrossRef]
11. Sereshti, H.; Amirafshar, A.; Kadi, A.; Nodeh, H.R.; Rezania, S.; Hoang, H.Y.; Barghi, A.; Vasseghian, Y. Isolation of organophosphate pesticides from water using gold nanoparticles doped magnetic three-dimensional graphene oxide. *Chemosphere* **2023**, *320*, 138065. [CrossRef]
12. Liu, T.; Li, D.; Huang, K.; Tan, S.; Huang, L. Preparation and water/oil separation of super-hydrophobic biomass adsorbent based on three-dimensional graphene aerogel. *J. Chem. Technol. Biotechnol.* **2023**, *98*, 744–755. [CrossRef]
13. Pan, D.; Ge, S.; Tian, J.; Shao, Q.; Guo, L.; Liu, H.; Wu, S.; Ding, T.; Guo, Z. Research progress in the field of adsorption and catalytic degradation of sewage by hydrotalcite-derived materials. *Chem. Rec.* **2020**, *20*, 355–369. [CrossRef] [PubMed]
14. Keerthi, M.; Manavalan, S.; Chen, S.M.; Shen, P.-W. A facile hydrothermal synthesis and electrochemical properties of manganese dioxide@ graphitic carbon nitride nanocomposite toward highly sensitive detection of nitrite. *J. Electrochem. Soc.* **2019**, *166*, B1245. [CrossRef]
15. Zheng, X.; Zhang, C.; Mao, D.; Mao, H.; Yu, J. Fabrication of MnCoO x composite oxides for catalytic CO oxidation via a solid-phase synthesis: The significant effect of the manganese precursor. *New J. Chem.* **2022**, *46*, 4343–4352. [CrossRef]
16. Tariq, H.A.; Abraham, J.J.; Shakoor, R.A.; Al-Qaradawi, S.; Karim, M.R.A.; Chaudhry, U. Synthesis of lithium manganese oxide nanocomposites using microwave-assisted chemical precipitation technique and their performance evaluation in lithium-ion batteries. *Energy Storage* **2020**, *2*, e202. [CrossRef]
17. Pandey, A.; Dalal, S.; Dutta, S.; Dixit, A. Structural characterization of polycrystalline thin films by X-ray diffraction techniques. *J. Mater. Sci. Mater. Electron.* **2021**, *32*, 1341–1368. [CrossRef]
18. Brundle, C.R.; Crist, B.V. X-ray photoelectron spectroscopy: A perspective on quantitation accuracy for composition analysis of homogeneous materials. *J. Vac. Sci. Technol.* **2020**, *38*, 041001. [CrossRef]
19. Han, X.X.; Rodriguez, R.S.; Haynes, C.L.; Ozaki, Y.; Zhao, B. Surface-enhanced Raman spectroscopy. *Nat. Rev. Methods Primers* **2022**, *1*, 87. [CrossRef]
20. Saadatkhah, N.; Carillo Garcia, A.; Ackermann, S.; Leclerc, P.; Latifi, M.; Samih, S.; Patience, G.S.; Chaouki, J. Experimental methods in chemical engineering: Thermogravimetric analysis—TGA. *Can. J. Chem. Eng.* **2020**, *98*, 34–43. [CrossRef]
21. Feng, D.; Guo, D.; Zhang, Y.; Sun, S.; Zhao, Y.; Shang, Q.; Tan, H. Functionalized construction of biochar with hierarchical pore structures and surface O-/N-containing groups for phenol adsorption. *Chem. Eng. J.* **2021**, *410*, 127707. [CrossRef]
22. Brand, C.; Kiałka, F.; Troyer, S.; Knobloch, C.; Simonović, K.; Stickler, B.A.; Hornberger, K.; Arndt, M. Bragg diffraction of large organic molecules. *Phys. Rev. Lett.* **2020**, *125*, 033604. [CrossRef]
23. Hou, X.; Zheng, Y.; Lv, S.; Ma, Z.; Ma, X. Effective removal of hexamethyldisiloxane using a citric acid modified three-dimensional graphene aerogel. *Renew. Energy* **2022**, *199*, 62–70. [CrossRef]
24. Yang, R.; Zhang, Q.; Li, C.; Zhang, J.; Xin, Y.; Ju, X.; Wang, D.; Shi, J.; Zheng, Y. Macroscopic liquid-like three-dimensional graphene oxide-based derivatives for efficient copper ion adsorption in water treatment. *J. Mater. Sci.* **2022**, *57*, 19756–19768. [CrossRef]
25. Hong, C.; Chen, K.; Zheng, X.; Wan, Y.; Li, Z.; Lin, L. Hierarchical porous structure of urushiol mediated Fe_3O_4/three-dimensional graphene composites towards enhanced Fenton degradation of tetracycline. *Chem. Eng. Sci.* **2023**, *281*, 119111. [CrossRef]
26. Ma, X.; Xu, Y. Three-dimensional porous nitrogen-doped carbon aerogels derived from cellulose@ mof for efficient removal of dye in water. *J. Environ. Chem. Eng.* **2022**, *10*, 108385. [CrossRef]
27. Motaghi, H.; Arabkhani, P.; Parvinnia, M.; Javadian, H.; Asfaram, A. Synthesis of a highly porous three-dimensional PVA/GO/ZIF-67 cryogel for the simultaneous treatment of water contaminated with cadmium (ii) and lead (ii) heavy metal ions. *New J. Chem.* **2022**, *46*, 4449–4461. [CrossRef]
28. Selvakumar, R.; Guhananthan, A.; Palanisami, T. Recent advances in micropollutant removal and mitigation from water using three dimensional adsorbent materials. *Curr. Opin. Environ. Sci. Health* **2023**, *2023*, 100475. [CrossRef]
29. Yang, F.; Zhang, J.; Lin, T.; Ke, L.; Huang, L.; Deng, S.-P.; Zhang, J.; Tan, S.; Xiong, Y.; Lu, M. Fabrication of waste paper/graphene oxide three-dimensional aerogel with dual adsorption capacity toward methylene blue and ciprofloxacin. *J. Iran. Chem. Soc.* **2023**, *20*, 801–816. [CrossRef]

30. Qu, H.; Xiao, X.; Han, Z.; Hu, M.; Shen, S.; Yang, L.; Jia, F.; Wang, T.; Ye, Z.; Sun, W.; et al. Graphene oxide nanofiltration membrane based on three-dimensional size-controllable metal–organic frameworks for water treatment. *ACS Appl. Nano Mater.* **2022**, *5*, 5196–5207. [CrossRef]
31. Zheng, A.L.T.; Ohno, T.; Andou, Y. Recent progress in photocatalytic efficiency of hybrid three-dimensional (3D) graphene architectures for pollution remediation. *Top. Catal.* **2022**, *65*, 1634–1647. [CrossRef]